Multimodal analysis of polyoxometalate/photosensitizer modified nanoporous block copolymers

Julian Kund[a§], Jan-Hendrik Kruse[b§], Ivan Trentin[c], Clarissa Read[d], Gregor Neusser[a] Andreas Gruber[a], Dominik Blaimer[a], Ulrich Rupp[d], Carsten Streb[c*], Kerstin Leopold[a], Felix H. Schacher[b*], Christine Kranz[a*]

[a]Institute of Analytical and Bioanalytical Chemistry, Ulm University, Albert-Einstein-Allee 11, 89081 Ulm, Germany

[b]Institute of Organic Chemistry and Macromolecular Chemistry, Friedrich-Schiller University Jena, Lessingstraße 8, 07743 Jena

[c]Institute of Inorganic Chemistry I, Ulm University, Albert-Einstein-Allee 11, 89081 Ulm

[d]Central Facility of Electron Microscopy, Ulm University, Albert-Einstein-Allee 11, 89081 Ulm

Abstract

Heterogeneous light-driven catalysis is a cornerstone of sustainable energy conversion schemes such as solar water splitting. However, to date most catalytic studies in the field focus on bulk analyses quantifying the amount of produced hydrogen and oxygen. Here, we report on *ex situ* and *operando* studies with micrometer to nanometer resolution of a heterogenized catalyst/photosensitizer system. As a model, the molecular photosensitizer $[Ru(bpy)_3]^{2+}$ and the molecular metal oxide water oxidation catalyst $[Co_4(H_2O)_2(PW_9O_{34})_2]^{10-}$ were co-immobilized within a nanoporous block copolymer membrane *via* electrostatic interactions. In a yet unprecedented approach, *operando* scanning electrochemical microscopy (SECM) allowed tracking the light induced oxygen evolution with spatial and temporal resolution. Complementary *ex situ* element analyses using micro-X-ray fluorescence (μXRF) and scanning transmission electron microscopy/x-ray energy dispersive spectroscopy (STEM/EDX) provided spatially resolved information on the local concentration and distribution of the molecular components.

Keywords

water oxidation catalysis, block copolymer membranes, heterogeneous photocatalysis, SECM, μXRF

1. Introduction

Heterogeneous catalysis is a cornerstone of modern chemical research, and most industrial chemical processes use one or more heterogeneous catalysts.[1] More recently, the field of sustainable energy has become one of the main drivers of heterogeneous catalyst development, as the splitting of water into hydrogen (H_2) and oxygen (O_2) is one of the major paths to carbon-neutral fuels.[2] One particularly promising approach to this end is artificial photosynthesis where chemical and materials solutions for light-driven water splitting are developed.[3,4] The concept relies on highly active and stable catalysts for the hydrogen evolution reaction (HER) and water oxidation catalysis (WOC).[5] Specifically, the 4-proton-4-electron WOC is a bottleneck, as suitable catalysts must combine high redox-activity and oxidative / hydrolytic stability with economic viability.[6] This has led to materials design approaches ranging from single-atom catalysts[7] to molecules,[8] clusters[9], nanoparticles[10] and bulk materials[6,11]. Independent of the type of catalyst, there is common consensus that industrial photo(electro)catalytic water splitting schemes require the use of heterogeneous or heterogenized catalysts to ensure their compatibility with large-scale technological deployments.[12] Thus, modern materials science is targeting the development of high-performance heterogeneous WOCs based on earth-abundant components,[5] embedding them in suitable supports. However, to-date, most heterogeneous or heterogenized WOC development relies on bulk reactivity analyses, such as quantification of the evolved O_2 in solution and/or the gas phase using fluorescence-based oxygen sensors,[13] head-space gas chromatography,[14] or Clark-type electrodes.[15] While this approach provides viable averaged (bulk) information on the performance of the catalyst (*i.e.* amount of O_2 evolved per gram of catalyst material), no information, *e.g.*, regarding the distribution and molecule-in-matrix stability of catalysts is obtained. Critical insights into the catalytic performance of reactive sites, *e.g.,* photosensitizer molecules or water oxidation sites, are not accessible by bulk methods. In addition, fundamental limitations of the material, *e.g.,* poor light-penetration into the bulk materials, inaccessibility of catalytic sites, inhomogeneous distribution of the active compounds, or major mass-transport limitations cannot be extracted from these bulk measurements. In this regard, we use scanning electrochemical microscopy (SECM) and correlate the SECM data with micro-X-ray fluorescence spectroscopy (μXRF) and scanning transmission electron microscopy/energy-dispersive X-ray spectroscopy (STEM/EDX). By this approach, we demonstrate how spatially and temporally resolved *in situ / operando* WOC reactivity data, kinetic information and *ex situ* information on spatial distribution can be obtained for molecular photosensitizer and molecular WOC systems heterogenized within nanoporous block copolymer membranes. The concept is inspired by ground-breaking

studies where SECM has been employed for H_2 / O_2 quantification at the surface of photocatalytic systems including $BiVO_4$-based semiconductors,[16] photoanodes,[17,18] cobaloxime HER catalysts,[19] and manganese-based WOC electrocatalysts.[20]

To explore the use of SECM in light-driven heterogenized WOC, we designed a model system utilizing the prototype ruthenium photosensitizer $[Ru(bpy)_3]^{2+}$ (= Ru-PS; bpy = 2,2'-bipyridine),[21] which features well-understood photophysics and is characterized by high oxidative redox-potentials capable of driving many WOCs. As WOC, we chose the polyoxometalate (POM) cluster $[Co_4(H_2O)_2(PW_9O_{34})_2]^{10-}$ (= POM-WOC),[22–24] whose WOC activity under a range of photochemical and electrochemical conditions has been explored, and where embedding in polymeric membranes has been reported recently.[25,26] For heterogenization of the active components, nanoporous membranes based on polystyrene-*block*-poly(2-(dimethylamino)ethyl methacrylate) (PS-*b*-DMAEMA) are used, where hydrophilic PDMAEMA units can be positively charged by protonation[27] to facilitate POM-WOC binding. In contrast, the hydrophobic polystyrene (PS) block provides a mechanically rigid membrane scaffold (Figure 1a).

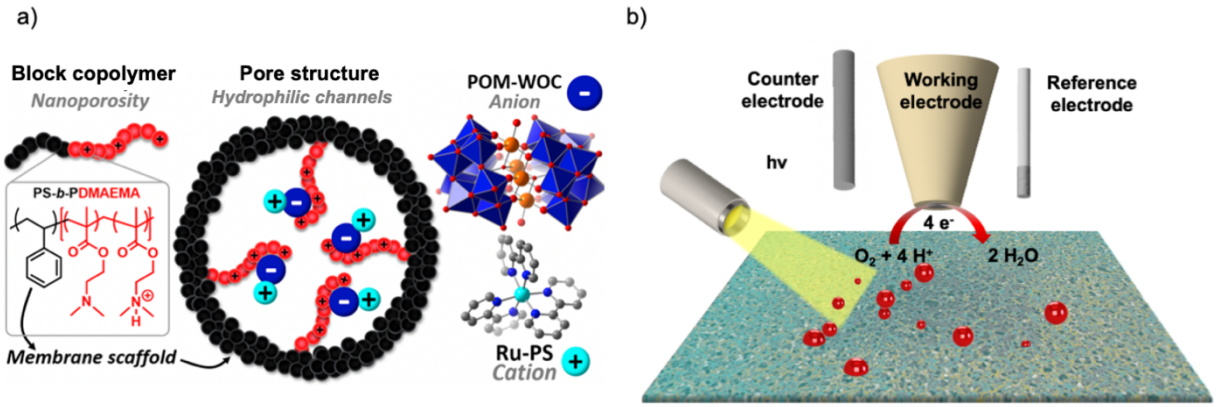

Figure 1: a) Schematic of the nanoporous block copolymer and heterogenized PS and WOC through electrostatic interactions. b) Schematic of local *operando* O_2 measurements within a nanoporous block copolymer membrane (SEM image using false colors) using SECM.

The resulting PS-*b*-PDMAEMA block copolymers were then fabricated into nanoporous membranes *via* the so-called NIPS (non-solvent induced phase separation) process.[28,29] This type of membrane has recently been successfully applied for the heterogenization of POM-based oxidation catalysts,[30] as well as Ru-PS and thiomolybdate catalysts for light-driven hydrogen evolution.[31] Anchoring of the photoactive components can be achieved through electrostatic[32,33] or covalent interactions.[34]

To the best of our knowledge, the present study reports the first spatially and temporally, *operando* O_2 measurements of soft matter-embedded molecular photoactive components, *i.e.*, hereafter referred to as WOCbranes. Instead of conventionally used bulk photocatalytic measurements. The latter may result in lower apparent O_2 values, as O_2 may be trapped within the

porous nanostructured membrane, and also they do not provide information on spatial and temporal reactivity differences of the heterogeneous system, as mass transport effects as well as heterogeneous component distribution are typically not observable *via* bulk measurements. Hence, a strategy was developed enabling the time-resolved quantification of O_2 in close proximity to the membrane surface using a customized SECM setup that allowed gentle purging with Ar to drive produced O_2 out of the membrane. In combination, with *ex-situ* element analysis by STEM/EDX, µXRF, and high resolution-contiunuum source-graphite furnance atomic absorption spectrometry (HR-CS-GFAAS) quantitative analysis of Co and Ru could be determined along with correlated information on homogeneity, morphology and molecular distribution of photosensitizer and catalyst.

2. Results and Discussion

The Ru-PS and POM-WOC were immobilized in PS-*b*-PDMAEMA block copolymer membranes via electrostatic interactions. PS-*b*-PDMAEMA was synthesized in a two-step procedure by anionic polymerization adapted from the literature.[35] In brief, the hydrophobic block was prepared *via* nitroxide-mediated polymerization (NMP) of styrene forming the membrane scaffold as depicted in **Figure S1**. In a second step, the PS macroinitiator was used for the NMP of DMAEMA, which led to the final block copolymer PS_{304}-*b*-$PDMAEMA_{71}$ (M_n= 42,900 g mol^{-1}, Đ=1.20, **Figure S2**); the subscripts denote the degree of polymerization in the respective segment. Nuclear magnetic resonance (NMR) measurements (**Figure S2a**) resulted in a weight fraction of 26 wt% of DMAEMA, which has an increased hydrophilic fraction compared to earlier studies.[27,31,36] **Figure S3** shows SEM micrographs of the block copolymer membrane, where the nanoporous nature is clearly visible. The anionic POM-WOC was anchored to the positively charged DMAEMA units by immersion of the membrane into an aqueous POM-WOC-containing solution (see Supporting Information). The anionic POM units (POM-WOC charge: -10) facilitate the subsequent immobilization of the cationic RuPS (see **Figure 1a** and Supporting Information for details). Thermogravimetric analysis gave approximate 38.8 wt-% POM-WOC and *ca.* 3.7 wt-% Ru-PS (**Figure S2c**). Based on earlier results and electrostatic considerations,[31] we assume that the relatively low Ru-PS loading observed is due to repulsive electrostatic interactions between Ru-PS and cationic PDMAEMA chains (**Figure 1a**).

Scanning electron microscopy (SEM) and transmission electron microscopy (TEM), respectively (see **Figure S2** and **Figure S4**) show the “sponge-like” morphology of the membrane with pores of varying size up to 20 – 30 µm (blue arrows), and varying shapes and density, which is in line with literature reports for this type of block copolymer membranes.[28,30,37] The “finger-like” or “rod-like” features with a thickness of *ca.* 50 – 60 nm

(red arrows) are associated with the block copolymer (**Figure S4b**,**d)**. The thickness of the membrane in the range of 52.5 to 55.4 µm, as determined via SEM and TEM cross-sectional images. For high-resolution STEM/EDX mapping of the distribution of Ru-PS and POM-WOC within the inner pores of the membrane, the WOCbranes were embedded within an EPON™ epoxy resin.[38] Thereby, artifacts due to sample preparation (*e.g.* vacuum drying) are avoided (for details see Supporting Information).

The dark fringes adjacent to the rod-like polymeric structures evident in the STEM image (Error! Reference source not found.**)** and TEM images (**Figure S4)** reveal the presence of heavy elements, which originate from the POM-WOC (W and Co) and from the Ru-PS (Ru). These are also clearly discernible in the EDX maps surrounding the rod-like features (*i.e.*, the carbon EDX map shown in **Figure S5** reflects the high carbon content of the rod-like polymer structures). The EDX maps show also the high oxygen content originating from $[Co_4(H_2O)_2(PW_9O_{34})_2]^{10-}$. The rod-shape and round features visible in the STEM image are related to the orientation of the polymer within the EPON resin and differences in the intensities of the dark fringes is likely related to the orientation and sectioning artifacts. The distribution of the mapped elements at the edges of the rod-like structures indicates the successful immobilization through electrostatic interactions between positively charged PDMAEMA and the negatively charged POM-WOCs.

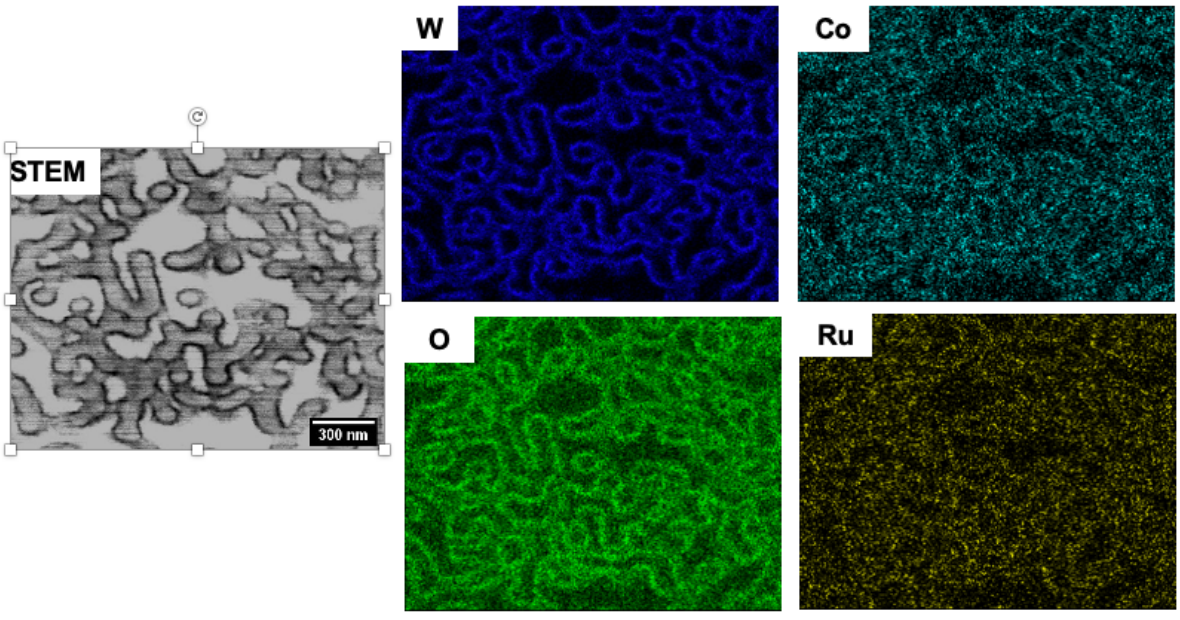

Error! Reference source not found.: STEM/EDX mapping of the elemental distribution of tungsten (W), cobalt (Co), oxygen (O), and ruthenium (Ru).

The element ratio of 0.26 for Co:W derived from the EDX data is in excellent agreement with the element ratio of the POM-WOC itself (Co:W = 0.22). For Ru ($[Ru(bpy)_3]^{2+}$), an unambiguous quantification from EDX data is difficult, as there is an overlap of the signals of Ru and Cl in

EDX mappings. The difference in energy between Cl (2.62 keV) and Ru (2.58 keV) is only 40 eV. Hence, with a detector resolution of around 130 eV a clear distinction is impeded.[39] The observed Cl signal (see **Figure S5**) originates from the $[Ru(bpy)_3]Cl_2$ counter-anions or may originate from residual NaCl used in the POM- WOC crystallization.[24] Consequently**,** the Ru content within the modified block copolymer membranes was determined *via* high resolution-continuum source-graphite furnance atomic absorption spectrometry (HR-CS-GFAAS) after digestion of small amounts of the WOCbranes. Ru concentrations in the range of nmol mm^{-2} were found (see below), varying among different immobilization batches and storage times of the membrane. An explanation may be that the positively charged DMAEMA fraction of the polymer counteracts the electrostatic interaction of the photosensitizer with the catalyst.

Next, we used *operando* SECM measurements to demonstrate that the WOCbranes show light-driven WOC activity and evolve O_2 under irradiation. Electrochemical O_2 measurements using microelectrodes have been proven to be a valuable way to determine photocatalytic activity as recently shown for strontiumtitanate ($SrTiO_3$).[40] We used static SECM measurements with Pt microelectrodes to quantitatively analyze the light-driven evolution of O_2 at a distance of 30 µm of the microelectrode to the membrane surface (for details on positioning the microelectrode at the membrane, see **Figure S6a**). A customized SECM cell was used, which facilitates illumination of the membrane (with a fibre-coupled LED (λ = 470 nm) and allows purging the membrane with Ar (i-t curves depicting the current response when the membrane is purged either with air (magenta) or Ar (grey) are shown in **Figure S8a**) . The membranes were purged (for approx. 15 min) prior to irradiation to remove any O_2 (below the detection limit of our measurements) from the membrane. During the photocatalytic measurements, a continuous Ar flow of 1 mL min^{-1} was maintained to drive the produced O_2 out the membrane as schematically depicted in **Figure S6b**. *Operando* O_2 measurements were performed in O_2-free borate buffer solution (pH 8.05) with $Na_2S_2O_8$ as sacrificial electron donor[41] in substrate generation/tip collection mode[42] applying a potential of −500 mV vs. Ag/AgCl at the SECM tip.

The pH dependence of the permeability of PDMAEMA membranes has been previously reported.[28] O_2 bubbles in the size range around 15 nm should completely pass the membranes at pH 6 – 10. During homogenous catalysis, it has been reported that in dependence of the concentrations of the catalyst $[Co_4(H_2O)_2(PW_9O_{34})_2]^{10-}$ the amount of O_2 concentration reached a plateau after 5-15 min of illumination.[43] We initially adapted this exposure time of 15 min, yet, applied intervals of 60 s irradiation for insight in the kinetic of the O_2 evolution. **Figure 1b** shows schematically the O_2 measurements under irradiation and **Figure 3a** exemplarily depicts the increase of cathodic current measured at the SECM tip originating from the reduction of O_2 during the individual irradiation steps (green curve). The same experiments were carried

out under dark conditions (magenta curve) and resulted, as expected, in a constant background current. The current response reveals an initially slow increase in O_2 evolution, which increases exponentially with illumination time – a behaviour that was observed for most of the examined WOCbranes (see **Figure S7a**). Exemplary i-t curves for continuous illumination for a WOCbrane and a non-modified block copolymer membrane are shown in **Figure S8b**, clearly indicating a current response only for the WOCbrane. Interestingly, after storage of the illuminated WOCbranes for several hours in ultrapure water, bubbles of oxygen were observed at the membrane surface as shown in **Figure S8c**. This is in contrast to homogeneous photocatalysis reported in the literature of the WOC-POM using the same sacrificial electron donor and photosensitizer,[43] although it should be noted that the reported O_2 measurements were obtained *via* head-space gas chromatography (GC). We hypothesize that the observed delayed onset might be still attributed to diffusion limitations within the membrane, which is dependent on the actual investigated area of the membrane. Areas with high polymer density may lead to the observed delay. Based on Faraday laws and assuming - for simplicity - a cylindrical volume given by the distance of the microelectrode to the membrane and the overall diameter of the microelectrode (active microwire and glass sheath), the O_2 concentration can be approximated. **Figure 3b** shows the obtained O_2 concentrations measured at two different immobilization batches (termed membrane 1 and membrane 2 here). It should be noted that the two different membranes were stored in ultrapure water for different times prior to the SECM measurements (see Supporting Information) and further *ex-situ* analytical characterization. The O_2 concentrations of the six samples were in the range of 163.37 to 386.15 µmol L^{-1} for a total illumination time of 15 min (see **Table S2**), indicating apparent variabilities between the individual samples. Also, **Figure S7b** shows the change in cathodic current measured under irradiation at a non-modified block copolymer membrane and at the two investigated immobilization batches.

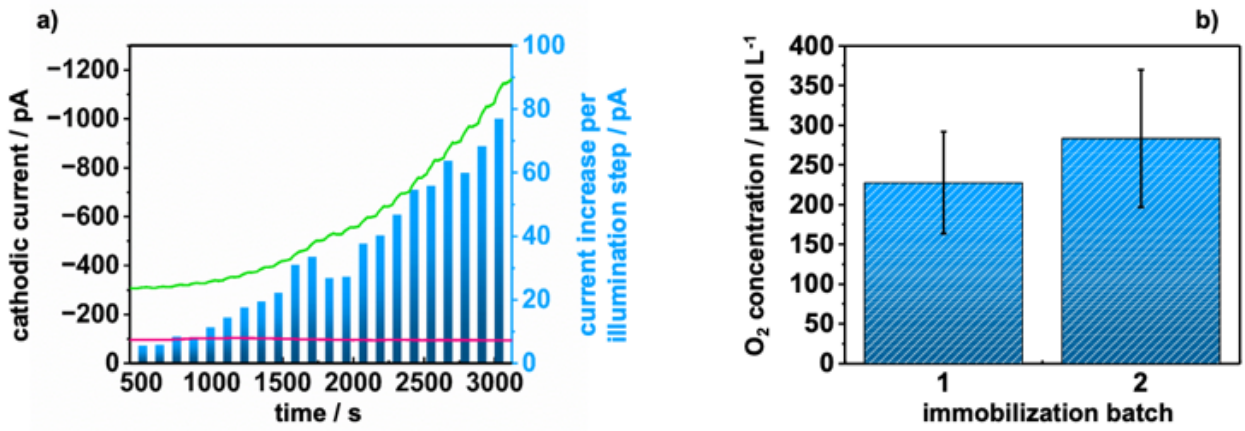

Figure 3: a) Exemplary current response recorded at the microelectrode during illumination (green, illumination was started after 500 s) and under dark conditions (magenta), (see Table S2, measurement

membrane 2.2). The current increase per illumination step is shown by the blue bars; b) O_2 concentration of two different immobilization batches with a total exposure time of 15 min (n=6).

The nature of this variability in the current response and the time of photocatalytic activity was further qualitatively and quantitatively analyzed with respect to the immobilized POM-WOC and Ru-PS content. We investigated, WOCbranes *via* EDX prior and after the *operando* light-driven catalytic measurements, as shown in **Figure S9**. A decrease in the W and Co EDX signal after illumination indicates that during catalysis, the WOC may undergo some degradation, which may be associated with the observed current decrease over time most observed over a period of 15 min for most *operando* SECM measurements.

Although, high-resolution STEM/EDX mappings (**Figure 2**) clearly show the presence of POM-WOC, the probed sample sections in these high-resolution maps cover an area of less than 2 μm^2, which is not representative for statistically meaningful evaluation of the macroscopic homogenity of WOC and Ru-PS in these molecule-in-matrix systems. This information is crucial for optimization of synthesis and loading procedures of the nanoporous block copolymer membranes to achieve high photocatalytic activity. Moreover, heterogeneities on a larger scale may explain the variations in the observed O_2 evolution, as the probed area in the SECM experiment is approx. 0.06 mm^2 giving the obverall dimension of the microelectrode and the distance to the membrane surface (*i.e.*, assuming a cylindrical configuration). As a novel non-destructive 2D elemental mapping method, µXRF remains scarsely used for soft materials,[44] gives access to element distribution maps of sample areas up to 20 x 30 cm, in a concentration range from low ppm up to wt.-%, and with a spatial resolution of about 25 µm; it is therefore ideally suited to study the elemental distribution of WOC-POM within the membranes on a macroscopic scale. **Figure 4** presents examplary intensity maps of W and Co of a WOCbrane with a size of 105.2 mm^2 or 3.1 mm^2, respectively from the immobilization batch A. Maps of another batch are presented in **Figure S10** and **Table S3**, respectively. W and Co were detected in both investigated membrane batches and evaluation of intensities revealed quite uniform distributions (see also **Figure S10**).

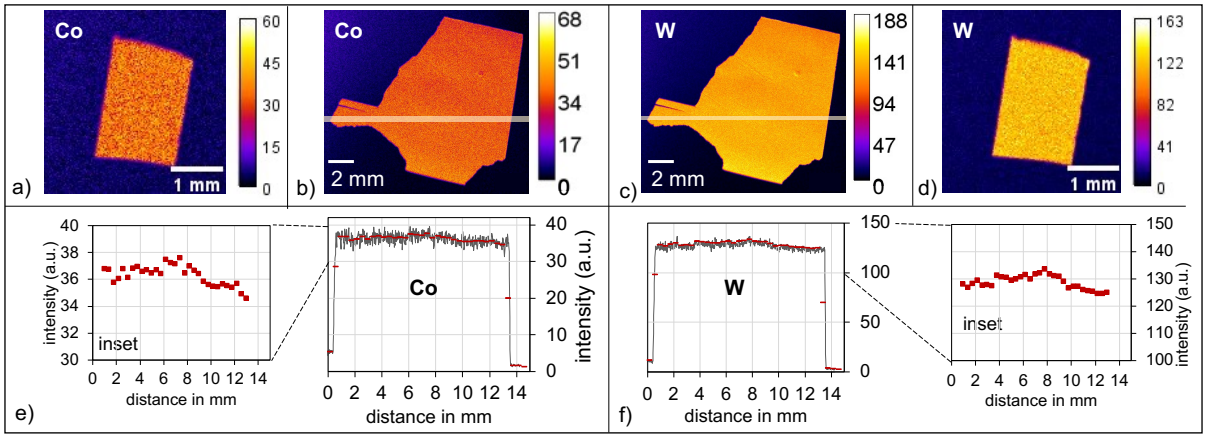

Figure 4: a) - d) Exemplary element maps and e), f) intensity distribution along the marked line of cobalt and tungsten in membrane 1. a), d) Sample size: 3.04 mm^2; b), e) sample size: 105.2 mm^2; c), f) relative intensities of Co/W along the 400 µm thick line marked in b), d): grey line: intensity at 25 µm resolution; red squares: mean values at 400 µm resolution.

To evaluate whether the observed variations in the element maps may influence the observed O_2 evolution, the resolution of the electrochemical measurement - providing a probing area of approximately 400 µm x 400 µm (0.16 mm^2) - was translated to this experiment. The intensity variation along a marked line (**Figure 4b, d**) was evaluated by calculation of mean intensities for 400 µm x 400 µm areas (**Figure 4e, f** red squares). As can be seen from the insets in Fig. 4e and 4f, the relative intensities differ only slightly, for Co between 34 and 38 a.u. and for W between 120 and 135 a.u., which confirms a quite uniform distribution of the WOC-POM within the membrane also on the macroscopic scale. To estimate the corresponding molar differences of Co as catalytically active element, quantitative analysis was performed. Several smaller pieces of a few mm^2 were obtained from membrane 1 (see **Figure S10a-c**) and after digestion, the Co content as well as the Ru content were quantitatively determined by GFAAS. The results are presented in **Table 2** (results for membrane 3 can be found in Supporting Information, **Table S3**). The Co and Ru content of the three investigated samples from membrane 1 resulted in similar concentrations for Co and Ru, respectively. The found mean Co content (for all three pieces) corresponds to 2.1 ± 0.6 nmol per probing area of 400 µm x 400 µm. Estimating now the observed variation width of 4 a.u. for Co results in ~0.3 nmol Co (~14.3%). However, it should be noted that this value is - due to the restricted sample number - within the range of precision of measurements but showing a clear trend. Thus, these minor inhomogeneities may slightly add to the observed variations in O_2 generation, however, most likely other effects, such as inhomogeneity in pore connectivity and/or limitations in diffusion might have a more pronounced affect.

Table 2: Concentration of Co and Ru determined by GFAAS measurement in digests of pieces of membrane 1. (Uncertainties given as ± one standard deviation with n=4 for concentrations and combined uncertainty for ratio.)

Sample	Size [mm^2]	Concentration found by GFAAS [nmol mm^{-2}]		Ratio Co / Ru
		Co	Ru	
1.1	3.04	14.3 ± 1.0	0.068 ± 0.015	210 ± 1
1.2	3.42	12.0 ± 2.3	0.057 ± 0.006	212 ± 2
1.3	5.66	13.8 ± 2.4	0.063 ± 0.003	219 ± 2

The element ratios of W and Co with ratios between 4.1 and 4.3, as determined by μXRF, fit well with the theoretical value of 4.5. The found averaged molar ratio of Co to Ru of 215 ± 4 suggests that only every 50th WOC-POM interacts electrostatically with a photosensitizer molecule. An explanation for this ratio may be that the positively charged PDMAEMA counteracts the electrostatic interaction of the photosensitizer with the catalyst. Despite this ratio of POM-WOC/Ru-PS and the fact that the heterogeneized system may lead to reduced light-penetration of the WOCbrane, significant light-driven catalytic activity as demonstrated by our SECM measurements, which may indicate a favorable, synergistic effect of the molecule-in-matrix system, compensating the relatively low loading of Ru-PS. It should be noted that for homogeneous photocatalysis in solution typically a significant excess of PS is used and typical concentration ratios of 0.002 – 0.01 CAT/Ru-PS are employed.[45,46]

Another aspect, which may contribute to the observed heterogeneity in activity is leaching during prolonged storage in solution. We observed varying Co contents for different membranes (Supporting Information **Table S3**). Hence, we investigated the effect of storage of a WOCbrane in ultrapure water for a period of 5 days. The obtained results confirm considerable and increasing concentrations of W and Co in the storage water (see **Figure S11**) indicating that also the content of WOC-POM varies with time. For SECM measurements, the membrane was usually stored in ultrapure water prior to the measurements (at least for 24 hours). It should be noted that the decrease in Co content in the storage water after 3 days is related to adsorption of Co at the walls of the storage container.

Conclusions

In conclusion, we demonstrated that POM-WOC catalysts and $[Ru(bpy)_3]^{2+}$ photosensitizers can be immobilized within nanoporous block copolymer membranes via electrostatic interactions resulting in photocatalytically active hybrid materials. Such block copolymer membranes are highly suitable matrices, as the degree of protonation of PDMAEMA and therefore POM-WOC / Ru-PS loadings can be controlled. A thorough characterization of these complex materials based on complementary analysis techniques facilitated obtaining unprecedented insight into the distribution of the WOC-POM and Ru-PS along with quantitative data on membrane loading and photocatalytic activity. Uniquely, SECM proved ideally suited for performing *operando* measurements of dissolved O_2 at WOCbranes probing sub-millimeter sized areas. Thus, obtained information on variations in O_2 evolution offered insight on the heterogeneity in WOC-POM/Ru-PS loading and membrane structure next to pore size and pore density. For high-performance heterogeneous WOCs, the macroscopic uniformity of the CAT/PS distribution is a prerequisite. μXRF element mapping provides access to the homogeneity of WOC elements within the membranes at a macroscopic scale. It was also shown that leaching effects need to be considered during extended storage periods. EDX

analysis of WOCbranes prior and after photocatalysis indicates a degradation/loss of the WOC, which may explain the observed decrease in photocatalytic activity with time. We present here the first successful measurements on such heterogenized WOC-POM modified nanoporous block copolymer membranes and to our best knowledge, no bulk measurements of such hybrid materials have been reported so far.

Acknowledgements

The authors acknowledge Prof. Paul Walther at the Central Facility for Electron Microscopy, Ulm University for his support. The authors acknowledge funding by the German Science Foundation (DFG) – Transregio-SFB – TRR234 “CataLight” project C4 and B3.

Keywords: water oxidation, polyoxometalates, block copolymer membranes, heterogeneous photocatalysis, SECM

[1] R. Schlögl, Heterogeneous Catalysis, Angew. Chemie Int. Ed. 54 (2015) 3465–3520. doi:10.1002/anie.201410738.

[2] B. Zhang, L. Sun, Artificial photosynthesis: opportunities and challenges of molecular catalysts, Chem. Soc. Rev. 48 (2019) 2216–2264. doi:10.1039/C8CS00897C.

[3] A. Listorti, J. Durrant, J. Barber, Solar to fuel, Nat. Mater. 8 (2009) 929–930. doi:10.1038/nmat2578.

[4] T. Faunce, S. Styring, M.R. Wasielewski, G.W. Brudvig, A.W. Rutherford, J. Messinger, A.F. Lee, C.L. Hill, H. DeGroot, M. Fontecave, D.R. MacFarlane, B. Hankamer, D.G. Nocera, D.M. Tiede, H. Dau, W. Hillier, L. Wang, R. Amal, Artificial photosynthesis as a frontier technology for energy sustainability, Energy Environ. Sci. 6 (2013) 1074. doi:10.1039/c3ee40534f.

[5] P. Du, R. Eisenberg, Catalysts made of earth-abundant elements (Co, Ni, Fe) for water splitting: Recent progress and future challenges, Energy Environ. Sci. 5 (2012) 6012. doi:10.1039/c2ee03250c.

[6] J. Li, C.A. Triana, W. Wan, D.P. Adiyeri Saseendran, Y. Zhao, S.E. Balaghi, S. Heidari, G.R. Patzke, Molecular and heterogeneous water oxidation catalysts: recent progress and joint perspectives, Chem. Soc. Rev. 50 (2021) 2444–2485. doi:10.1039/d0cs00978d.

[7] X.-F. Yang, A. Wang, B. Qiao, J. Li, J. Liu, T. Zhang, Single-Atom Catalysts: A New Frontier in Heterogeneous Catalysis, Acc. Chem. Res. 46 (2013) 1740–1748. doi:10.1021/ar300361m.

[8] S. Berardi, S. Drouet, L. Francàs, C. Gimbert-Suriñach, M. Guttentag, C. Richmond, T. Stoll, A. Llobet, Molecular artificial photosynthesis, Chem. Soc. Rev. 43 (2014) 7501–7519. doi:10.1039/C3CS60405E.

[9] A. Sartorel, M. Bonchio, S. Campagna, F. Scandola, Tetrametallic molecular catalysts for photochemical water oxidation, Chem. Soc. Rev. 42 (2013) 2262–2280. doi:10.1039/C2CS35287G.

[10] S. Ye, C. Ding, M. Liu, A. Wang, Q. Huang, C. Li, Water Oxidation Catalysts for Artificial Photosynthesis, Adv. Mater. 31 (2019) 1902069. doi:10.1002/adma.201902069.

[11] C. Costentin, D.G. Nocera, Self-healing catalysis in water, Proc. Natl. Acad. Sci. 114 (2017) 13380–13384. doi:10.1073/pnas.1711836114.

[12] S. Jiao, X. Fu, S. Wang, Y. Zhao, Perfecting electrocatalysts via imperfections: towards the large-scale deployment of water electrolysis technology, Energy Environ. Sci. 14 (2021) 1722–1770. doi:10.1039/D0EE03635H.

[13] F.L. Huber, S. Amthor, B. Schwarz, B. Mizaikoff, C. Streb, S. Rau, Multi-phase real-time monitoring of oxygen evolution enables: In operando water oxidation catalysis studies, Sustain. Energy Fuels 2 (2018) 1974–1978. doi:10.1039/c8se00328a.

[14] B. Limburg, E. Bouwman, S. Bonnet, Rate and Stability of Photocatalytic Water Oxidation using $[Ru(bpy)_3]^{2+}$ as Photosensitizer, ACS Catal. 6 (2016) 5273–5284. doi:10.1021/acscatal.6b00107.

[15] A. Indra, P.W. Menezes, M. Driess, Photocatalytic and photosensitized water splitting: A plea for well-defined and commonly accepted protocol, Comptes Rendus Chim. 21 (2018) 909–915. doi:10.1016/j.crci.2018.03.013.

[16] H. Ye, H.S. Park, A.J. Bard, Screening of Electrocatalysts for Photoelectrochemical Water Oxidation on W-Doped $BiVO_4$ Photocatalysts by Scanning Electrochemical Microscopy, J. Phys. Chem. C 115 (2011) 12464–12470. doi:10.1021/jp200852c.

[17] S. Chen, S. Prins, A. Chen, Patterning of BiVO 4 Surfaces and Monitoring of Localized Catalytic Activity Using Scanning Photoelectrochemical Microscopy, ACS Appl. Mater. Interfaces 12 (2020) 18065–18073. doi:10.1021/acsami.9b22605.

[18] F. Conzuelo, K. Sliozberg, R. Gutkowski, S. Grützke, M. Nebel, W. Schuhmann, High-

Resolution Analysis of Photoanodes for Water Splitting by Means of Scanning Photoelectrochemical Microscopy, Anal. Chem. 89 (2017) 1222–1228. doi:10.1021/acs.analchem.6b03706.

[19] E. Oswald, A. Gaus, J. Kund, M. Küllmer, J. Romer, S. Weizenegger, T. Ullrich, A.K. Mengele, L. Petermann, R. Leiter, P.R. Unwin, U. Kaiser, S. Rau, A. Kahnt, A. Turchanin, M. Delius, C. Kranz, Cobaloxime Complex Salts: Synthesis, Patterning on Carbon Nanomembranes and Heterogeneous Hydrogen Evolution Studies, Chem. – A Eur. J. 27 (2021) 1–9. doi:10.1002/chem.202102778.

[20] Z. Jin, A.J. Bard, Surface Interrogation of Electrodeposited MnO x and $CaMnO_3$ Perovskites by Scanning Electrochemical Microscopy: Probing Active Sites and Kinetics for the Oxygen Evolution Reaction, Angew. Chemie Int. Ed. 60 (2021) 794–799. doi:10.1002/anie.202008052.

[21] V. Balzani, P. Ceroni, A. Credi, M. Venturi, Ruthenium tris(bipyridine) complexes: Interchange between photons and electrons in molecular-scale devices and machines, Coord. Chem. Rev. 433 (2021) 213758. doi:10.1016/j.ccr.2020.213758.

[22] N. Li, J. Liu, B. Dong, Y. Lan, Polyoxometalate-Based Compounds for Photo- and Electrocatalytic Applications, Angew. Chemie. 132 (2020) 20963–20977. doi:10.1002/ange.202008054.

[23] D. Gao, I. Trentin, L. Schwiedrzik, L. González, C. Streb, The Reactivity and Stability of Polyoxometalate Water Oxidation Electrocatalysts, Molecules 25 (2019) 157. doi:10.3390/molecules25010157.

[24] Q. Yin, J.M. Tan, C. Besson, Y. V Geletii, D.G. Musaev, A.E. Kuznetsov, Z. Luo, K.I. Hardcastle, C.L. Hill, A Fast Soluble Carbon-Free Molecular Water Oxidation Catalyst Based on Abundant Metals, Science 328 (2010) 342–345. doi:10.1126/science.1185372.

[25] Z. Han, A.M. Bond, C. Zhao, Recent trends in the use of polyoxometalate-based material for efficient water oxidation, Sci. China Chem. 54 (2011) 1877–1887. doi:10.1007/s11426-011-4442-4.

[26] S. Herrmann, C. Ritchie, C. Streb, Polyoxometalate – conductive polymer composites for energy conversion, energy storage and nanostructured sensors, Dalt. Trans. 44 (2015) 7092–7104. doi:10.1039/C4DT03763D.

[27] F. Schacher, T. Rudolph, F. Wieberger, M. Ulbricht, A.H.E. Müller, Double Stimuli-Responsive Ultrafiltration Membranes from Polystyrene- block -poly(N , N -dimethylaminoethyl methacrylate) Diblock Copolymers, ACS Appl. Mater. Interfaces 1

(2009) 1492–1503. doi:10.1021/am900175u.

[28] F. Schacher, M. Ulbricht, A.H.E. Müller, Self-Supporting, Double Stimuli-Responsive Porous Membranes From Polystyrene- block -poly(N , N -dimethylaminoethyl methacrylate) Diblock Copolymers, Adv. Funct. Mater. 19 (2009) 1040–1045. doi:10.1002/adfm.200801457.

[29] K.-V. Peinemann, V. Abetz, P.F.W. Simon, Asymmetric superstructure formed in a block copolymer via phase separation, Nat. Mater. 6 (2007) 992–996. doi:10.1038/nmat2038.

[30] I. Romanenko, M. Lechner, F. Wendler, C. Hörenz, C. Streb, F.H. Schacher, POMbranes: polyoxometalate-functionalized block copolymer membranes for oxidation catalysis, J. Mater. Chem. A. 5 (2017) 15789–15796. doi:10.1039/C7TA03220J.

[31] I. Romanenko, A. Rajagopal, C. Neumann, A. Turchanin, C. Streb, F.H. Schacher, Embedding molecular photosensitizers and catalysts in nanoporous block copolymer membranes for visible-light driven hydrogen evolution, J. Mater. Chem. A 8 (2020) 6238–6244. doi:10.1039/D0TA01059F.

[32] M. Bonchio, M. Carraro, M. Gardan, G. Scorrano, E. Drioli, E. Fontananova, Hybrid photocatalytic membranes embedding decatungstate for heterogeneous photooxygenation, Top. Catal. 40 (2006) 133–140. doi:10.1007/s11244-006-0115-5.

[33] M. Bonchio, M. Carraro, G. Scorrano, E. Fontananova, E. Drioli, Heterogeneous Photooxidation of Alcohols in Water by Photocatalytic Membranes Incorporating Decatungstate, Adv. Synth. Catal. 345 (2003) 1119–1126. doi:10.1002/adsc.200303076.

[34] X. Zhang, P. Tanner, A. Graff, C.G. Palivan, W. Meier, Mimicking the cell membrane with block copolymer membranes, J. Polym. Sci. Part A Polym. Chem. 50 (2012) 2293–2318. doi:10.1002/pola.26000.

[35] W.A. Phillip, R.M. Dorin, J. Werner, E.M. V. Hoek, U. Wiesner, M. Elimelech, Tuning Structure and Properties of Graded Triblock Terpolymer-Based Mesoporous and Hybrid Films, Nano Lett. 11 (2011) 2892–2900. doi:10.1021/nl2013554.

[36] C. Hörenz, C. Pietsch, A.S. Goldmann, C. Barner-Kowollik, F.H. Schacher, Phase Inversion Membranes from Amphiphilic Diblock Terpolymers, Adv. Mater. Interfaces 2 (2015) 1500042. doi:10.1002/admi.201500042.

[37] Y. Wang, Nondestructive Creation of Ordered Nanopores by Selective Swelling of

Block Copolymers: Toward Homoporous Membranes, Acc. Chem. Res. 49 (2016) 1401–1408. doi:10.1021/acs.accounts.6b00233.

[38] E. BLAAUW, J. OOSTERBAAN, J. SCHAKENRAAD, Improved Epon embedding for biomaterials, Biomaterials 10 (1989) 356–358. doi:10.1016/0142-9612(89)90079-3.

[39] J.. J. Friel, X-Ray And Image Analysis in Electron Microscopy, Second Edi, Princeton Gamma-Tech, 2005.

[40] T. Kosaka, Y. Teduka, T. Ogura, Y. Zhou, T. Hisatomi, H. Nishiyama, K. Domen, Y. Takahashi, H. Onishi, Transient Kinetics of O 2 Evolution in Photocatalytic Water-Splitting Reaction, ACS Catal. 10 (2020) 13159–13164. doi:10.1021/acscatal.0c04115.

[41] A.L. Kaledin, Z. Huang, Y. V Geletii, T. Lian, C.L. Hill, D.G. Musaev, Insights into Photoinduced Electron Transfer between $[Ru(bpy)_3]^{2+}$ and $[S_2O_8]^{2-}$ in Water: Computational and Experimental Studies, J. Phys. Chem. A 114 (2010) 73–80. doi:10.1021/jp908409n.

[42] L. Johnson, D.A. Walsh, Tip generation–substrate collection–tip collection mode scanning electrochemical microscopy of oxygen reduction electrocatalysts, J. Electroanal. Chem. 682 (2012) 45–52. doi:10.1016/j.jelechem.2012.06.024.

[43] Z. Huang, Z. Luo, Y. V. Geletii, J.W. Vickers, Q. Yin, D. Wu, Y. Hou, Y. Ding, J. Song, D.G. Musaev, C.L. Hill, T. Lian, Efficient Light-Driven Carbon-Free Cobalt-Based Molecular Catalyst for Water Oxidation, J. Am. Chem. Soc. 133 (2011) 2068–2071. doi:10.1021/ja109681d.

[44] J.-C. Müller, M. Horstmann, L. Traeger, A.U. Steinbicker, M. Sperling, U. Karst, μXRF and LA-ICP-TQMS for quantitative bioimaging of iron in organ samples of a hemochromatosis model, J. Trace Elem. Med. Biol. 52 (2019) 166–175. doi:10.1016/j.jtemb.2018.12.012.

[45] B. Schwarz, J. Forster, M.K. Goetz, D. Yücel, C. Berger, T. Jacob, C. Streb, Visible-Light-Driven Water Oxidation by a Molecular Manganese Vanadium Oxide Cluster, Angew. Chemie Int. Ed. 55 (2016) 6329–6333. doi:10.1002/anie.201601799.

[46] J.W. Vickers, H. Lv, J.M. Sumliner, G. Zhu, Z. Luo, D.G. Musaev, Y. V Geletii, C.L. Hill, Differentiating homogeneous and heterogeneous water oxidation catalysis: confirmation that $[Co_4(H_2O)_2(\alpha\text{-}PW_9O_{34})2]^{10-}$ is a molecular water oxidation catalyst., J. Am. Chem. Soc. 135 (2013) 14110–8. doi:10.1021/ja4024868.